Ab initio calculations of the CaF$_2$ electronic structure and *F* centers

H. Shi, R. I. Eglitis, and G. Borstel

Fachbereich Physik, Universität Osnabrück, D-49069 Osnabrück, Germany

We present and discuss the results of calculations of the CaF$_2$ bulk and surface electronic structure. These are based on the *ab initio* Hartree-Fock method with electron correlation corrections and on density-functional theory calculations with different exchange-correlation functionals, including hybrid exchange techniques. Both approaches use the localized Gaussian-type basis set. According to our calculations the *ab initio* Hartree-Fock method considerably overestimates (20.77 eV) the optical band gap, whereas the density-functional calculations based on the Kohn-Sham equation with a number of exchange-correlation functionals, including local-density approximation (8.72 eV), generalized gradient approximations by Perdew and Wang (8.51 eV), and Perdew, Burke, and Ernzerhof (8.45 eV) underestimate it. Our results show that the best agreement with experiment (12.1 eV) can be obtained using a hybrid Hartree-Fock and density-functional theory exchange functional, in which Hartree-Fock exchange is mixed with density-functional theory exchange functionals, using Beckes three-parameter method, combined with the nonlocal correlation functionals by Perdew and Wang (10.96 eV). We also present calculations of CaF$_2$ (111), (110), and (100) surfaces. Our calculated surface energies confirm that the CaF$_2$ (111) surface is the most stable one, in agreement with the experiment. The characterization of *F* centers in CaF$_2$ is still a question of debate. In order to understand the behavior of the material with respect to its optical properties, we performed *ab initio* calculations to determine the electronic structure, atomic geometry, and formation energy of *F* center in CaF$_2$.

I. INTRODUCTION

Considering the high technological importance of CaF$_2$, it is not surprising, that during the last years, it has been the subject of many experimental and theoretical studies.[1–14] Fluorite CaF$_2$ is a cubic *Fm*3*m* large-gap insulator. The unit cell includes three ions, one cation chosen as origin, and two anions that are situated at $\left(\frac{1}{4}a, \frac{1}{4}a, \frac{1}{4}a\right)$ and $\left(\frac{3}{4}a, \frac{3}{4}a, \frac{3}{4}a\right)$, where *a* is the lattice constant. The experimental lattice constant for CaF$_2$ is 5.4630 Å.[15] Today, a large amount of experimental information on CaF$_2$ has been accumulated,[6,16–18] which requires an interpretation from the standpoint of the band structure of this crystal. Experimentally, the direct band gap is 12.1 eV[5] and the indirect gap is estimated to be 11.8 eV.[5]

The electronic structure of CaF$_2$ has been recently calculated from first principles and published by several research groups. In the beginning of the 1990s, Catti *et al.*[9] performed an all-electron *ab initio* Hartree-Fock (HF) calculation for the band structure of CaF$_2$. The energy-gap width between valence and conduction bands at the Γ point was about 21 eV, considerably exceeding the experimental value.

From another side, it is well known that the local-density and generalized-gradient approximations (GGA) to density-functional theory (DFT) systematically underestimate the band gap in semiconductors and insulators; an error of a factor 2 is typical. For example, in Ref. 4 the indirect band gap ($X \rightarrow \Gamma$) of 7.07 eV is underestimated with respect to experiment as expected in a GGA-DFT calculation. A similar result for the indirect band gap in CaF$_2$ (6.53 eV) using the first-principles orthogonalized linear combination of atomic orbitals (OLCAO) method in the local-density approximation (LDA) was obtained by Gan *et al.*[7]

Contemporary knowledge of defects in solids has helped to create a field of technology, namely, *defect engineering*, which is aimed at manipulating the nature and concentration of defects in a material so as to tune its properties in a desired manner or to generate different behavior. CaF$_2$ could become an important optical material if one could avoid or, at least, control the photoinduced defect formation, which thus far in applications degrades its optical quality. Therefore, it is important to understand the nature of defects in CaF$_2$.

Two intrinsic color centers have been observed in CaF$_2$ by electron spin-resonance techniques. One is the V_k, or self-trapped hole, whose resonance has been reported by Hayes and Twidell[19] in x-rayed CaF$_2$ at liquid-nitrogen temperatures (LNT). The other is the *F* center, an electron trapped in an anion vacancy, whose resonance has been found by Arends[20] in additively colored crystals and correlated with an optical absorption band at 3.3 eV.

To get a reliable basis for defect calculations, which requires a precise description of the optical band gap, we calculated the electronic structure of bulk CaF$_2$ by means of *ab initio* calculations based on the HF and DFT methods. We also present, in a second part of the paper, theoretical investigations for pure CaF$_2$ (111), (110), and (100) surfaces. These calculations will form the basis for future defect calculations in the surface region of CaF$_2$. In this work, by using the first principles calculations, we determine the electronic structure, atomic geometry, and formation energy of the *F* center in CaF$_2$.

II. METHOD OF CALCULATIONS

All numerical calculations dealing with the CaF$_2$ electronic structure were performed by the CRYSTAL computer

TABLE I. Optimized lattice constant a_o, and bulk modulus B for CaF_2.

Method	LDA	PWGGA	PBE	BLYP	B3PW	B3LYP	HF	Exp. Ref. 30 and 31
a_o (Å)	5.34	5.51	5.52	5.56	5.50	5.52	5.52	5.46
B (GPa)	103	88	90	79	85	91	93	82.71

code.[21] In our calculations we used several quite different methods: Hartree-Fock with different density functional theory (DFT) type *a posteriori* electron correlation corrections to the total energy,[22] such as generalized gradient approximation, Perdew-91 (HFPer91), Lee-Yang-Parr (HFLYP), and full-scale DFT calculations based on the Kohn-Sham equations with a number of exchange-correlation functionals, including local density approximation, GGA by Perdew and Wang (PW), Perdew, Burke, and Ernzernhof (PBE), as well as Becke exchange functionals using Beckes three-parameter method, combined with the nonlocal correlation functionals by Perdew and Wang, as those by Lee, Yang, and Parr (B3LYP). The CRYSTAL code uses the localized Gaussian-type basis set. In our calculations for CaF_2 we applied the basis set developed by Catti *et al.*[9] and used a modified conjugate gradient algorithm[23,24] to optimize the atomic coordinates and locate minima on the potential-energy surface (PES).

We performed band-structure calculations with $8 \times 8 \times 8$ $=512$ k points in the Brillouin zone (BZ). The calculation thresholds N (i.e., the calculation of integrals with an accuracy of 10^{-N}) were chosen as a compromise between the accuracy of the calculations and the large computational time for large cells. They are 7, 8, 7, 7, and 14 for the Coulomb overlap, Coulomb penetration, exchange overlap, the first-exchange pseudo-overlap, and for the second-exchange pseudo-overlap, respectively.[25] The convergence criteria for the self-consistent field (SCF) energy and eigenvalues were set to 10^{-10} and 10^{-12} a.u., respectively. An additional advantage of the CRYSTAL code is that it treats isolated two-dimensional (2D) slabs, without an artificial periodicity in the z direction perpendicular to the surface, and thereby is a very convenient tool for modeling of CaF_2 surfaces.

Unlike the (111) neutral surface, the problem in modeling the (100) polar surface is that it consists of charged planes F-F or Ca. If one assumes fixed ionic charges F^-, and Ca^{2+} (which is the case for shell model calculations), then modeling of the (100) surface exactly as would be obtained from a perfect-crystal cleavage leads either to an infinite macroscopic dipole moment perpendicular to the surface, when the slab is terminated by planes of different kinds (F_2 and Ca), or

to an infinite charge, when it is terminated by the same type of crystalline planes (F_2-F_2 or Ca-Ca). It is known that such crystal terminations make the surface unstable.[26,27] In real quantum-mechanical calculations for a finite-thickness slab terminated by the different kind of planes, the charge redistribution near the surface arising during the self-consistent-field procedure, could, in principle, compensate the macroscopic dipole moment. On the other hand, in the calculations of slabs terminated by similar planes, the charge neutrality could be easily retained by setting in the computer input an appropriate number of electrons or just put the net charge of the unit cell to zero. However, careful studies[26,28,29] demonstrate that these two options are energetically expensive with respect to the dipole moment elimination via introduction of vacancies. This is why in our calculations we removed half the F atoms from the F_2-terminated CaF_2 (100) surface.

To simulate F centers, we started with a 48-atom supercell with one of the fluorine atoms removed. After the fluorine atom is removed, the atomic configuration of the surrounding atoms is reoptimized via a search of the total energy minimum as a function of the atomic displacements from the regular lattice sites.

In order to have an accurate description of the F center, a basis set has been added at the fluorine vacancy, corresponding to the *ghost* atom. For the *ghost* atom, we used the same basis set as that used for the F^- ions of the bulk CaF_2.

III. RESULTS OF CALCULATIONS

A. CaF$_2$ bulk electronic structure

As a starting point of our calculations, we have tested how different methods reproduce the experimentally observable bulk properties—lattice constant a_o and the bulk modulus B.[30,31] The LDA calculations underestimate a_o by 2.2% and overestimate B by 24.5%. The HF method without any correlation corrections to the total energy overestimates both a_o (by 1.1%) and B (by 12.4%). HF with GGA corrections overestimates a_o by 0.9% and B by 6.4%. Lastly, the hybrid B3PW method gives the best result for the lattice constant a_o (overestimates only by 0.7%) and also for B (overestimates by 2.7%) (see Table I).

TABLE II. Static (Mulliken) charges of atoms and bond populations (in me) for bulk CaF_2 calculated by various methods.

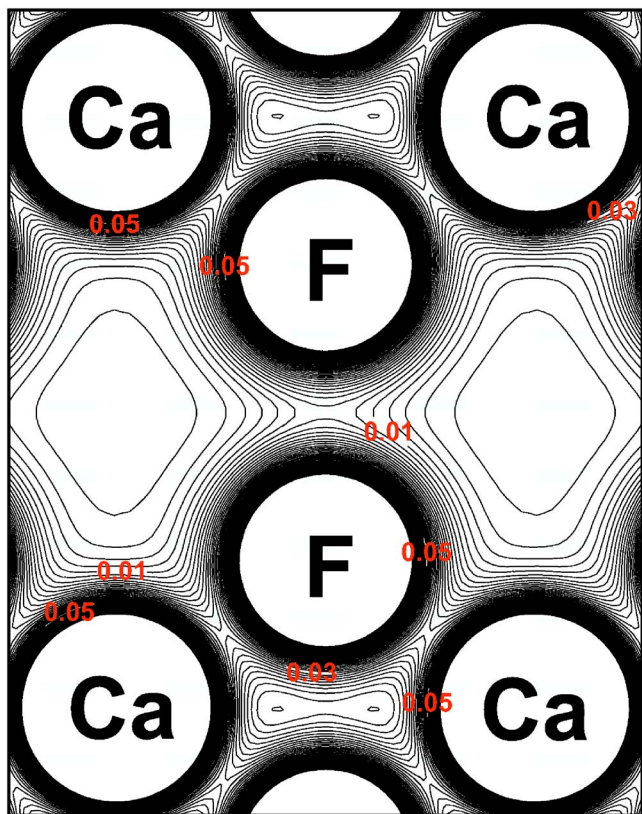| Atom	Charge Q (e) Bond pop. P (me)	LDA	PWGGA	PBE	BLYP	B3PW	B3LYP	HF
Ca^{2+}	Q	+1.728	+1.769	+1.771	+1.776	+1.803	+1.805	+1.895
F^-	Q	−0.864	−0.885	−0.886	−0.888	−0.902	−0.903	−0.948
F-Ca	P	−28	−8	−6	−8	−10	−12	−18
F-F	P	−38	−20	−18	−18	−22	−22	−24

FIG. 1. (Color online) Charge density map of CaF$_2$ bulk from (110) side view calculated by means of hybrid B3PW method. Isodensity curves are drawn from 0 to 0.1 e/bohr^3 with an increment of 0.002 e/bohr^3.

Table II presents results for the effective atomic charges and bond populations. The effective charges for Ca and F ions, both in the bulk and on the surface, turn out to be only slightly smaller than the formal ionic charges ($+2\ e$ and $-e$, respectively). This arises due to the high ionic nature of the Ca-F chemical bonding. Note that these results are close for all methods used. The most obvious difference is between the effective charges for the Ca ion calculated by LDA ($+1.728e$) and HF ($+1.895e$). Obviously, there is practically

TABLE III. The calculated optical gap (in electron volts) for the CaF$_2$ bulk. Experimentally the direct band gap is 12.1 eV[5] and the indirect band gap is equal to 11.8 eV[5].

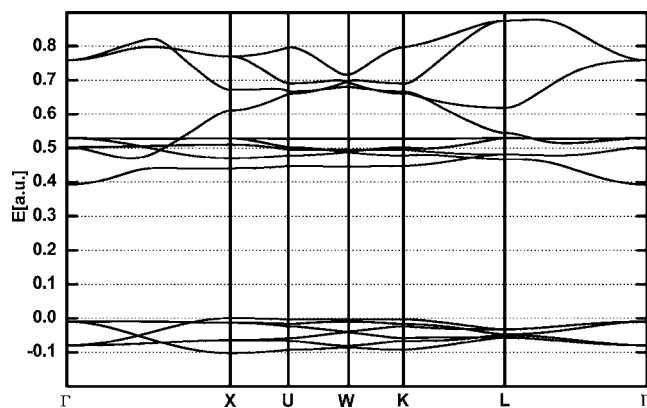| Optical gap	LDA	PWGGA	PBE	BLYP	B3PW	B3LYP	HF
Γ-Γ	8.72	8.51	8.45	8.40	10.96	10.85	20.77
X-X	9.30	9.33	9.30	9.28	11.99	11.93	22.72
U-U	9.60	9.58	9.55	9.52	12.27	12.20	23.07
W-W	9.56	9.55	9.52	9.49	12.23	12.16	23.00
L-L	11.41	10.82	10.77	10.64	13.63	13.54	24.90
X-Γ	8.44	8.22	8.20	8.16	10.68	10.57	20.43
U-Γ	8.55	8.34	8.29	8.24	10.78	10.67	20.53
W-Γ	8.54	8.33	8.28	8.24	10.78	10.66	20.55
L-Γ	9.34	9.07	9.02	8.96	11.58	11.46	21.50

FIG. 2. Electronic band structure of CaF$_2$ bulk calculated by means of the hybrid B3PW method.

no chemical bonding between Ca-F or F-F, since the relevant bond populations are even negative. Figure 1 shows the charge density map of CaF$_2$ bulk from the (110) side view obtained with the B3PW method. Figure 1 confirms that the charge density between atoms is very small in agreement with the charge and bond population calculations, reflecting the high degree of ionic bonding in this crystal.

Experimentally, the direct band gap for CaF$_2$ bulk is 12.1 eV[5] and the indirect band gap is estimated to be 11.8 eV[5]. It is a well-known fact that DFT-LDA calculations underestimate the band gap by a factor of typically two. According to our calculations, the indirect band gap ($X\to\Gamma$) using the LDA to the DFT is 8.44 eV (see Table III), considerably less as obtained experimentally. On the other hand, the band gap obtained through pure-HF calculations usually greatly overestimates the experimental value.[25] Indeed, results of our pure-HF calculations for indirect band gap ($X\to\Gamma$) (20.43 eV) confirm this rule (see Table III). A possible solution of this problem is the use of so-called hybrid functionals (a combination of the nonlocal HF exchange, DFT exchange, and the generalized gradient approximation correlation functional). Examples are so-called B3PW and B3LYP, which nowadays are extremely popular in quantum chemistry of molecules and recently have been applied to periodic-structure *ab initio* calculations of a wide range of crystalline materials.[32] It turns out that results obtained by the hybrid exchange techniques B3PW are in the best agreement with available experimental data for ABO$_3$ perovskites and their surfaces.[33–37] Also for the CaF$_2$ band structure, the hybrid B3PW and B3LYP methods gives the best results (see Table III). Namely, according to our calculations, the indirect band gap ($X\to\Gamma$) using B3PW is 10.68 eV (see Fig. 2), and 10.57 eV by the B3LYP functional, in good agreement with experiment.

The upper valence band consists of F p orbitals, whereas the conduction band bottom consists essentially of Ca d orbitals. The orbital contribution from F atoms is small in this energy range (see Fig. 3).

B. Atomic and electronic structure of CaF$_2$ (111), (110), and (100) surfaces

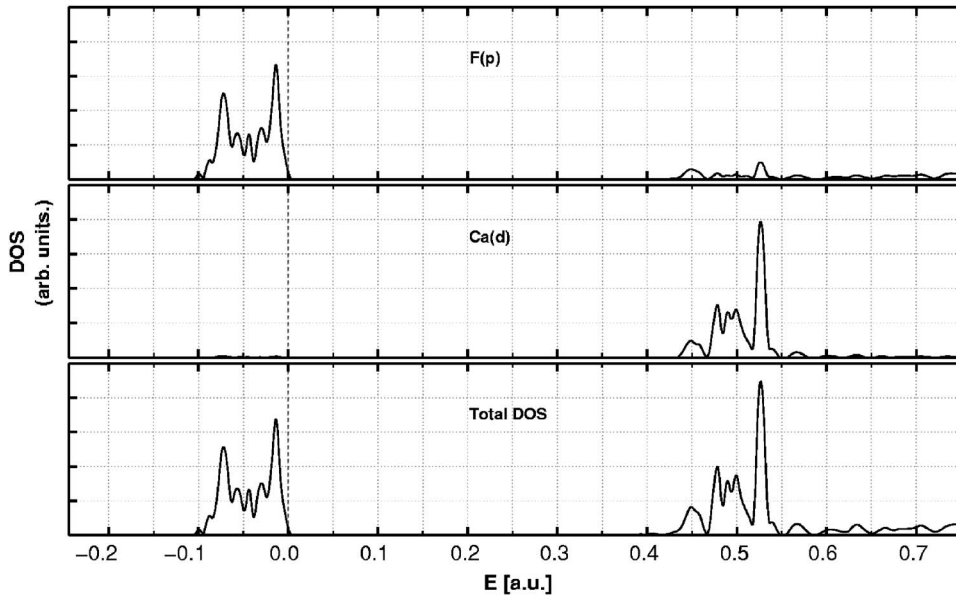We started our calculations from the case of the CaF$_2$ (111) surface, which is known to be experimentally stable.

FIG. 3. The calculated total and projected density of states for CaF_2 bulk by means of hybrid B3PW method.

Let us, for the analysis, look at the particular B3PW results, since they gave the best agreement with experiment for the lattice constant and bulk modulus. The structure of the CaF_2 (111) surface and directions of atomic displacements is illustrated in Fig. 4. We found, in contrast to Puchin *et al.*,[12] that the atomic displacements for the (111) surface is not fully negligible. The calculated displacements of the atoms by the HF method are <0.01 Å in Ref. 12, whereas according to our B3PW calculations F atoms in the upper sublayer of the top (111) surface layer are relaxed inward by 0.05 Å (see Table IV).

As a next step, we optimized the slab atomic structure for the case of the CaF_2 (110) surface. We performed the geometry relaxation for a slab containing 15 layers (see Table V). For the CaF_2 (110) surface there appears an additional degree of freedom for the atomic displacements in the direction Y (see Fig. 5). Ca atoms at the CaF_2 (110) surface upper layer move inward (toward the bulk) by 3.35% of lattice constant a_o, whereas the displacement of upper layer Ca atoms in the case of CaF_2 (111) termination was only 0.68% of a_o toward the bulk. Also for the deeper layers, the magnitudes of the atomic displacements in the case of CaF_2 (110) surface is considerably larger than for the CaF_2 (111) surface, see Tables IV and V for comparison.

Next, we calculated the relaxation of the CaF_2 (100) surface using a slab containing 15 layers (see Fig. 6). We found, that relaxation of CaF_2 (100) surface is considerably stronger than for (111) and (110) surfaces. F atoms at the upper surface layer are relaxed most noticeably, by 5.65% of a_o toward the bulk, but also F atoms even at seventh layer are still considerably displaced, by 0.82% a_o inward and by 0.76% of lattice constant a_o outward (see Table VI).

FIG. 4. (Color online) Schematic sketch of CaF_2 (111) surface structure. Layer numbering introduced in this figure is used in Table IV. Arrows indicate the calculated displacement directions of Ca and F atoms.

TABLE IV. Atomic relaxation of CaF_2 slab containing nine layers in (111) direction (in percent of the lattice constant), calculated by means of hybrid B3PW method. Positive sign corresponds to outward atomic displacement (toward the vacuum).
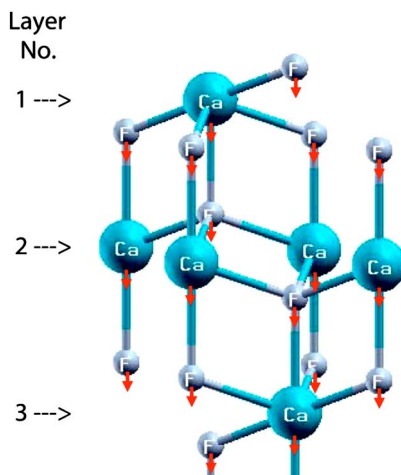
Layer	Atom	B3PW $\Delta z(\%)$
1	F	−0.90
	Ca	−0.68
	F	−0.78
2	F	−0.34
	Ca	−0.41
	F	−0.36
3	F	−0.34
	Ca	−0.28
	F	−0.23
4	F	−0.19
	Ca	−0.14
	F	−0.09
5	F	−0.05
	Ca	0
	F	0.05

TABLE V. Atomic relaxation of CaF$_2$ slab containing 15 layers in (110) direction, calculated by means of hybrid B3PW method. ΔY is the relative displacement (in percents of a_o) between two F atoms. Negative sign means the shortening of the F-F distance.

Layer	Atom	B3PW $\Delta y(\%)$	B3PW $\Delta z(\%)$
1	F	+3.21	−0.87
	Ca	0	−3.35
2	F	−0.14	−0.83
	Ca	0	+0.80
3	F	+0.08	−0.26
	Ca	0	−0.88
4	F	−0.03	−0.40
	Ca	0	−0.13
5	F	+0.03	−0.22
	Ca	0	−0.33
6	F	−0.03	−0.18
	Ca	0	−0.13
7	F	+0.03	−0.08
	Ca	0	−0.09

The cation effective charges using the B3PW hybrid method in two top CaF$_2$ (111) surface layers (+1.797 e) and (+1.802 e) turn out to be smaller than in the bulk (+1.803 e), whereas the F charges (−0.891 e) in the upper sublayer of the top surface layer is by 0.011 e larger than in
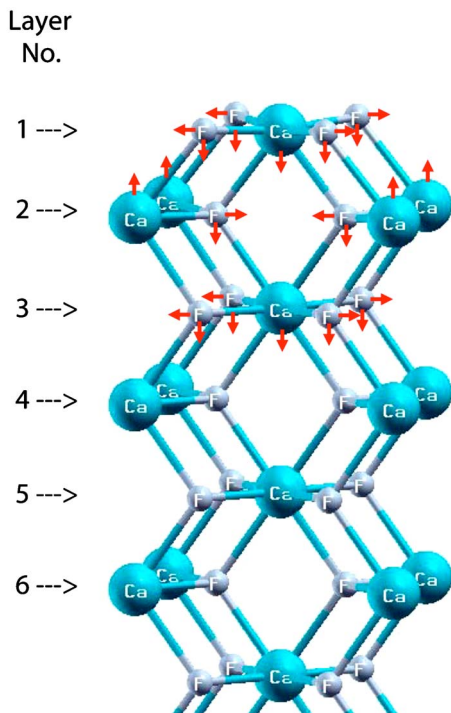

Layer No.

FIG. 5. (Color online) Schematic sketch of CaF$_2$ (110) surface structure. For CaF$_2$ surface there appears an additional degree of freedom in the Y direction for atomic displacements. Arrows indicate the calculated displacement directions of Ca and F atoms.
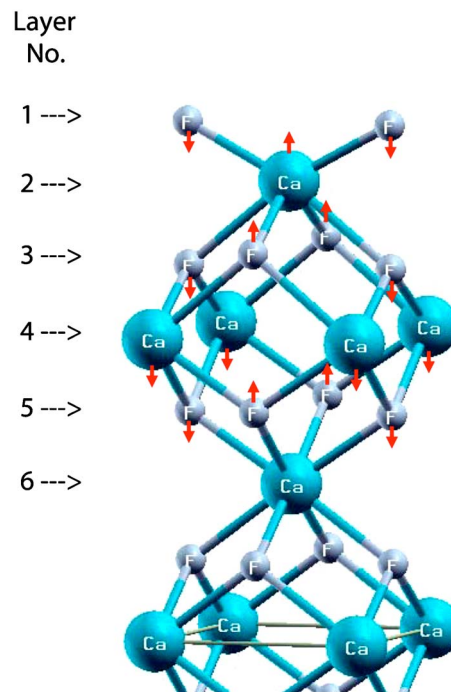

Layer No.

FIG. 6. (Color online) Schematic sketch of CaF$_2$ (100) surface structure. Layer numbering introduced in this figure is used in Table VI. Arrows indicate the calculated displacement directions of Ca and F atoms.

the bulk (−0.902 e). Changes in the atomic charges in the deeper layers become very small. Bond population analysis between atoms for the CaF$_2$ (111) surface shows that the major effect observed here is a strengthening of the Ca-F chemical bond near the surface. The bond population between Ca and F atoms in the upper sublayer of the first surface layer by (+12 me) exceeds the respective bond population value between Ca and F atoms in the bulk. At deeper layers of the CaF$_2$ (111) surface, the bond population between Ca and F atoms is practically the same as in the bulk. The similar effect, strengthening of the Ti-O chemical bond

TABLE VI. Atomic relaxation of CaF$_2$ slab containing 15 layers in (100) direction (in percent of the lattice constant), calculated by means of the hybrid B3PW method. Positive sign corresponds to outward atomic displacement (toward the vacuum).

Layer	Atom	B3PW$\Delta z(\%)$
1	F	−5.63
2	Ca	+0.34
3	F	−3.20
	F	+4.03
4	Ca	−0.03
5	F	+1.49
	F	−1.53
6	Ca	−0.07
7	F	−0.82
	F	+0.76

TABLE VII. The calculated direct $(\Gamma \to \Gamma)$ optical gap (in electron volts) for the CaF_2 (100), (110), and (111) slabs. All calculations have been performed using hybrid B3PW method. The last column contains the respective optical gap for the CaF_2 bulk.

CaF_2 slabs	(100)	(110)	(111)	CaF_2 bulk
Direct $(\Gamma \to \Gamma)$ optical gap	9.95	10.13	10.87	10.96

near the $SrTiO_3$ (001) surface, was observed by us also for $SrTiO_3$.[33]

The charge of the CaF_2 (110) surface upper-layer F atom is $-0.882e$ and increases by 0.02 e in comparison to the bulk, and by 0.009 e relatively to the CaF_2 (111) surface upper-layer F atom. The largest charge change is for the CaF_2 (110) surface upper-layer Ca atom. Its charge is reduced by -0.041 e in comparison to the bulk charge $(+1.803$ $e)$ and is equal to $+1.762$ e. Charges in CaF_2 (110) surface deeper layers become very close to the relevant Ca and F charges in the bulk.

Static Mulliken charges of atoms for the CaF_2 (100) surface containing 15 layers calculated by the hybrid B3PW method differ from the bulk charges by $+0.055$ e for the F and by -0.052 e for the Ca, which is considerably more than in the cases of CaF_2 (110) and (111) surfaces. We can observe an increase of the Ca-F bond population near the CaF_2 (100) surface by $(+18$ me$)$ in comparison to the CaF_2 bulk and thereby a strengthening of the Ca-F chemical bonding. The strengthening of the Ca-F chemical bonding between Ca and F atoms in the upper surface layer is more pronounced for the CaF_2 (100) surface than for the CaF_2 (111) termination.

We also computed the electronic energy-band structures for the CaF_2 (100), (110), and (111) surfaces using the B3PW method. As we can see from the main results collected in Table VII, the direct optical band gap for the (111) surface (10.87 eV) is close to the relevant optical band gap value for the CaF_2 bulk (10.96 eV). The direct optical band gaps for CaF_2 (100) and (110) surfaces (9.95 and 10.13 eV) are considerably reduced in comparison to the CaF_2 bulk.

The calculated density of states (DOS) for the CaF_2 (100) surface shows that the (100) surface upper-layer F(p) orbitals move upward, toward the Fermi energy, with respect to the F(p) orbitals at deeper levels, and this leads to the narrowing of the (100) surface band gap. This finding is in line with the narrowing of the band gap at $SrTiO_3$, $BaTiO_3$, and $PbTiO_3$ perovskite (100) surfaces reported by us in Refs. 33–35 and by Padilla and Vanderbilt for $SrTiO_3$ and $BaTiO_3$ (Refs. 38 and 39) (100) surfaces.

The calculated DOS for the CaF_2 (110) surface shows that the (110) surface first layer F(p) atomic orbitals have some states near the Fermi energy, but their magnitude is rather small. Thereby they contribute to some narrowing of the band gap, but this effect is not so well pronounced than in the case of the CaF_2 (100) surface.

From the calculated DOS for the CaF_2 (111) surface we can conclude that the F(p) atomic orbitals in the upper layer of the CaF_2 (111) surface have one large peak near the Fermi energy, whereas the F(p) DOS has two peaks at deeper lay-

TABLE VIII. Surface energies for CaF_2 (111), (110), and (100) surfaces calculated by means of the hybrid B3PW method.

CaF_2 Slabs	Number of Layers	B3PW Surface Energies (J/m^2)	Exp. Surface Energy (J/m^2) (Ref. 40)
(111)	9	0.438	0.45 J/m^2
	7	0.437	—
(110)	15	0.719	—
	9	0.717	—
(100)	15	0.979	—
	9	0.957	—

ers, and with a growing number of layers, they become more and more close to the relevant F(p) DOS for the CaF_2 bulk.

C. Surface energies

Next we discuss the surface energetics. The surface energy was calculated as

$$E_{\text{surface}} = \frac{1}{2}[E_{\text{slab}}^{(\text{relax})} - nE_{\text{bulk}}], \tag{1}$$

where n is the number of bulk primitive cells in the slab. E_{bulk} is the total energy per bulk unit cell, and $E_{\text{slab}}^{(\text{relax})}$ is the total energy for a relaxed slab containing n layers. Our calculated surface energies for CaF_2 (111), (110), and (100) surfaces containing a different number of layers, using the hybrid B3PW functional, are collected in Table VIII. As we can see from the results of our calculations, the (111) surface energy is the lowest (0.437 J/m^2) for the slab containing seven layers, thereby indicating that the (111) surface is the most stable, in agreement with the experiment, and practically does not depend on the number of layers in the slab. For the slab containing nine layers, according to our calculations, the surface energy is practically the same
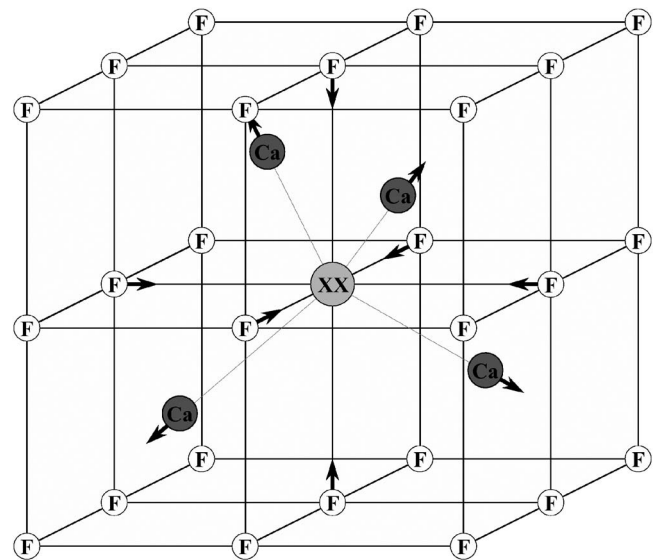

FIG. 7. A view of the *F*-center nearest-neighbor geometry with the indication of relaxation shifts. The position of the color center is indicated by XX.

TABLE IX. Formation energy, $E^{\text{form}}(F)$ (in electron volts), for F center calculated by B3PW and HF methods for different supercells.

Number of atoms	B3PW $E^{\text{form}}(F)$ (eV)	HF $E^{\text{form}}(F)$ (eV)
12	7.88	6.73
24	7.87	6.73
48	7.87	6.73

(0.438 J/m^2). The calculated (111) surface energy is close to the (111) surface energy calculated earlier by Puchin *et al.*,[12] using the *ab initio* Hartree-Fock method, and is in good agreement with the only experimental estimation to our knowledge available (0.45 J/m^2).[40]

Our calculated surface energy for the (110) surface is considerably larger (0.719 J/m^2) than for the (111) surface. Finally, our calculations show that the surface energy for the (100) surface is the largest one (0.979 J/m^2) and also agrees qualitatively with the only previous *ab initio* (HF) calculation mentioned in Ref. 12 (1.189 J/m^2).

D. *F* center in CaF$_2$

To estimate the formation energy of the fluorine vacancy in CaF$_2$ crystal, we used the following expression:

$$E^{\text{form}}(F) = E(\text{Fluorine}) + E(F) - E(\text{perfect}), \quad (2)$$

where $E(\text{Fluorine})$ is the energy for the isolated fluorine atom, $E(F)$ and $E(\text{perfect})$ the energies of the defective crystal containing the F center (see Fig. 7) and the perfect crystal, respectively. The fluorine vacancy formation energy, calculated using the B3PW method, going from the 12 atomic supercells to 48 atomic supercells, as shown in Table IX, is reduced only by 0.01 eV and equals to 7.87 eV for the supercell containing 48 atoms.

The analysis of the effective charges of atoms surrounding the F center shows that the electron associated with the removed fluorine atom is well localized ($-0.752\ e$) (see Table X) inside the fluorine vacancy (V_F), $-0.04e$ is localized on the four nearest Ca atoms and $-0.09\ e$ is localized on the 6 s nearest-neighbor fluorine atoms. The charge-density map of the F center in CaF$_2$ shows (see Fig. 8) that in CaF the charge is well localized inside the V_F. The F center spin density, calculated using the B3PW method, is 0.716 e and 0.827 e according to our calculations by the HF method.
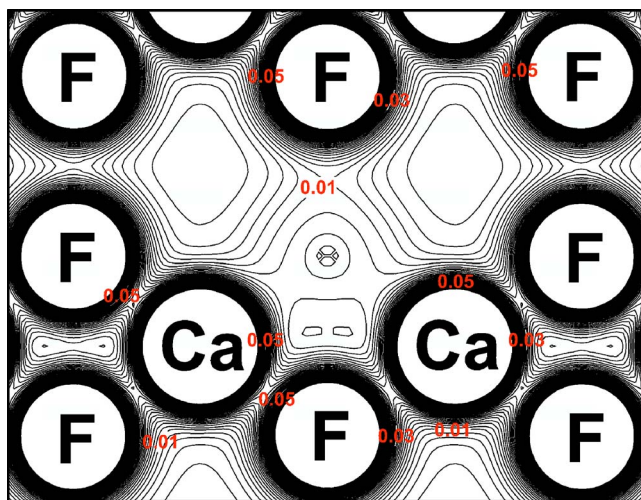

FIG. 8. (Color online) Charge-density map of CaF$_2$ crystal with the periodic F center from the (110) side view. Isodensity curves are drawn from 0 to 0.1 e/bohr^3 with an increment of 0.002 e/bohr^3.

The positions of 10 atoms surrounding the F center (see Fig. 7) after lattice relaxation to the minimum of the total energy are given in Table XI. The conclusion is that the four nearest Ca atoms are displaced outward of the F center by 0.15% a_o, as follows from the B3PW calculations, and by 0.16% a_o outward according to our HF calculations. These small displacements of atoms near the F center in CaF$_2$ can be explained by the fact that the F-center charge in CaF$_2$ is close to the fluorine charge in CaF$_2$ bulk (see Table X).

The defect-defect coupling is also seen in the CRYSTAL-B3PW calculations. The width of the *defect band* is 1.13 eV for the 12-atom supercells, 0.23 eV for the 24-atom supercells and 0.07 eV for the 48-atom supercells (see Fig. 9). In these supercells the distance between the periodically repeated F centers varies from 5.50 Å (12 atoms) to 9.53 Å (48 atoms). The F-center band for the 48-atom supercell in the Γ point lies 6.75 eV above the top of the valence band (see Fig. 9).

As mentioned in the introduction, CaF$_2$ exhibits optical absorption at 3.3 eV. Our results for defect levels suggest a possible mechanism for this absorption. The observed optical absorption may correspond to an electron transition from the F-center ground state, which lies 6.75 eV above the top of the valence band, to the conduction band. The F-center defect band at Γ point is located 4.24 eV (see Fig. 9) under the

TABLE X. The effective charges of the F center and surrounding atoms in the CaF$_2$ bulk calculated by the hybrid B3PW method for a supercell containing 48 atoms.

Atom(i)	B3PW Q(e)	HF Q(e)	B3PWΔQ(e)	HFΔQ(e)	B3PW Spin($n_\alpha - n_\beta$) (e)	HF Spin($n_\alpha - n_\beta$) (e)
XX	−0.752	−0.835	+0.150	+0.113	0.716	0.827
Ca(1)	+1.793	+1.890	−0.010	−0.005	0.035	0.020
F(2)	−0.917	−0.962	−0.015	−0.014	0.019	0.014
F(3)	−0.902	−0.948	0	0	0.001	0
Ca(4)	+1.802	+1.896	−0.001	+0.001	0	0
F(5)	−0.902	−0.949	0	−0.001	0.003	0.001

TABLE XI. Relaxation of 10 atoms surrounding the F center placed at the coordinate origin.

n-th nearest	Atom	Number	B3PWΔz(%)	HFΔz(%)
1	Ca	4	+0.15	+0.16
2	F	6	−0.28	−0.11

conduction band, which is close to the experimentally observed absorption energy of 3.3 eV.

IV. CONCLUSIONS

Summing up, a comparison of *ab initio* HF and DFT calculations employing different exchange-correlation functionals clearly demonstrates that the best agreement with experiment for the lattice constant, bulk modulus, as well as the band structure is possible to achieve by the hybrid B3PW functional. According to our calculations, the direct band gap for CaF$_2$ bulk (10.96 eV) is narrowed for the (111) (10.87 eV), (110) (10.13 eV), and (100) (9.95 eV) surfaces. The CaF$_2$ (111) surface energy, according to our calculations, is the smallest one (0.437 J/m^2), indicating that the (111) surface is the most stable, in good agreement with the available experimental result.

The characterization of native point defects in CaF$_2$ has important technological implications. In this work, we applied a first-principles approach to the calculations of F centers in CaF$_2$. We found, that the vacancy formation energy in CaF$_2$ is 7.87 eV. The charge-density map of the F center in
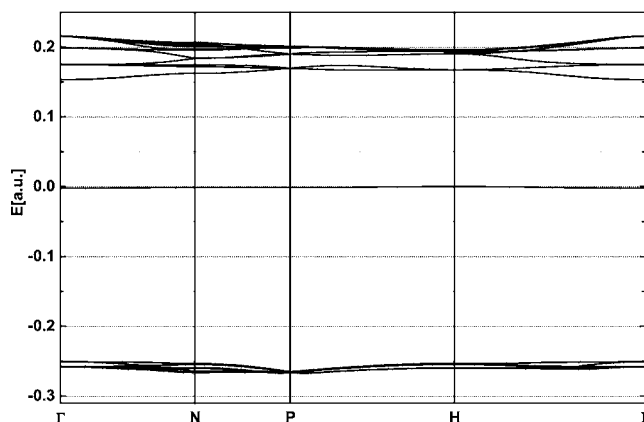

FIG. 9. Calculated band structure for the 48-atom supercell modeling the F center.

CaF$_2$ shows, that the charge is well localized inside the V_O. The F-center spin density, calculated using the B3PW method, is 0.716e. The relaxation of atoms surrounding the F center, according to our calculations, is small. Our results for F-center defect levels suggests a possible mechanism for explanation of the optical absorption observed experimentally in CaF$_2$ at 3.3 eV.

[1] K. Schmalzl, D. Strauch, and H. Schober, Phys. Rev. B **68**, 144301 (2003).

[2] N. H. de Leeuw and T. G. Cooper, J. Mater. Chem. **13**, 93 (2003).

[3] N. H. de Leeuw, J. A. Purton, S. C. Parker, G. W. Watson, and G. Kresse, Surf. Sci. **452**, 9 (2000).

[4] M. Verstraete and X. Gonze, Phys. Rev. B **68**, 195123 (2003).

[5] G. W. Rubloff, Phys. Rev. B **5**, 662 (1972).

[6] J. Barth, R. L. Johnson, M. Cardona, D. Fuchs, and A. M. Bradshaw, Phys. Rev. B **41**, R3291 (1990).

[7] F. Gan, Y. N. Xu, M. Z. Huang, W. Y. Ching, and J. G. Harrison, Phys. Rev. B **45**, 8248 (1992).

[8] W. Y. Ching, F. Gan, and M. Z. Huang, Phys. Rev. B **52**, 1596 (1995).

[9] M. Catti, R. Dovesi, A. Pavese, and V. R. Saunders, J. Phys.: Condens. Matter **3**, 4151 (1991).

[10] A. S. Foster, C. Barth, A. L. Shluger, R. M. Nieminen, and M. Reichling, Phys. Rev. B **66**, 235417 (2002).

[11] A. Jockisch, U. Schröder, F. W. Wette, and W. Kress, J. Phys.: Condens. Matter **5**, 5401 (1993).

[12] V. E. Puchin, A. V. Puchina, M. Huisinga, and M. Reichling, J. Phys.: Condens. Matter **13**, 2081 (2001).

[13] M. Merawa, M. Lunell, R. Orlando, M. Gelize-Duvignau, and R. Dovesi, Chem. Phys. Lett. **368**, 7 (2003).

[14] A. V. Puchina, V. E. Puchin, E. A. Kotomin, and M. Reichling,

Solid State Commun. **106**, 285 (1998).

[15] R. W. G. Wyckoff, *Crystal Structures*, 9th Ed. (Interscience/John Wiley, New York, 1963), Vol. 1.

[16] P. Camy, J. L. Doualan, S. Renard, A. Braud, V. Menard, and R. Moncorge, Opt. Commun. **236**, 395 (2004).

[17] G. A. Kumar, R. Riman, S. C. Chae, Y. N. Jang, I. K. Bae, and H. S. Moon, J. Appl. Phys. **95**, 3243 (2004).

[18] T. Tsujibayashi, K. Toyoda, S. Sakuragi, M. Kamada, and M. Itoh, Appl. Phys. Lett. **80**, 2883 (2002).

[19] W. Hayes and J. W. Twidell, Proc. Phys. Soc. London **79**, 1295 (1962).

[20] J. Arends, Phys. Status Solidi **7**, 805 (1964).

[21] V. R. Saunders, R. Dovesi, C. Roetti, M. Causa, N. M. Harrison, R. Orland, and C. M. Zicovich-Wilson, *CRYSTAL-2003 User Manual* (University of Torino, Italy, 2003).

[22] M. Causa and A. Zupan, Chem. Phys. Lett. **220**, 145 (1994).

[23] H. B. Schlegel, J. Comput. Chem. **3**, 214 (1982).

[24] B. Civalleri, P. D'Arco, R. Orlando, V. R. Saunders, and R. Dovesi, Chem. Phys. Lett. **348**, 131 (2001).

[25] C. Pisani (ed.), *Quantum-Mechanical Ab initio Calculations of the Properties of Crystalline Materials*, Lecture Notes in Chemistry, Vol. 67 (Springer, Berlin, 1996).

[26] C. Noguera, J. Phys.: Condens. Matter **12**, R367 (2000).

[27] P. W. Tasker, J. Phys. C **12**, 4977 (1979).

[28] A. Pojani, F. Finocchi, and C. Noguera, Surf. Sci. **442**, 179 (1999).

[29] F. Bottin, F. Finocchi, and C. Noguera, Phys. Rev. B **68**, 035418 (2003).

[30] R. C. Weast (ed), *CRC Handbook of Chemistry and Physics* (CRC Press, Boca Raton, 1976).

[31] M. Nicolav, J. Cryst. Growth **218**, 62 (2000).

[32] J. Muscat, A. Wander, and N. M. Harrison, Chem. Phys. Lett. **342**, 397 (2001).

[33] E. Heifets, R. I. Eglitis, E. A. Kotomin, J. Maier, and G. Borstel, Phys. Rev. B **64**, 235417 (2001).

[34] E. Heifets, R. I. Eglitis, E. A. Kotomin, J. Maier, and G. Borstel, Surf. Sci. **513**, 211 (2002).

[35] R. I. Eglitis, S. Piskunov, E. Heifets, E. A. Kotomin, and G. Borstel, Ceram. Int. **30**, 1989 (2004).

[36] S. Piskunov, E. A. Kotomin, E. Heifets, J. Maier, R. I. Eglitis, and G. Borstel, Surf. Sci. **575**, 75 (2005).

[37] S. Piskunov, E. Heifets, R. I. Eglitis, and G. Borstel, Comput. Mater. Sci. **29**, 165 (2004).

[38] J. Padilla and D. Vanderbilt, Surf. Sci. **418**, 64 (1998).

[39] J. Padilla and D. Vanderbilt, Phys. Rev. B **56**, 1625 (1997).

[40] J. J. Gilman, J. Appl. Phys. **31**, 2208 (1960).